Available online at www.sciencedirect.com

ScienceDirect

Procedia CIRP 141 (2026) 280–285

www.elsevier.com/locate/procedia

10th Conference on High Performance Cutting (CIRP-HPC 2026)

Surface-Ply Defect Quantification in Machined UD GFRP Composites

Matthias Nutte[a*], Edouard Rivière-Lorphèvre[a], Valentin Dambly[a,b], Pedro-José Arrazola[c], Ismail Lazoglu[d], Aurélie Granjon[e], François Ducobu[a]

[a]*Machine Design and Production Engineering Lab, Research Institute for Science and Material Engineering, UMONS, Mons 7000, Belgium*
[b]*IDEKO, Dynamics & Control departement, Arriaga kalea 2, E-20870 Elgoibar, Spain*
[c]*Mechanical and Manufacturing Department, Faculty of Engineering, Mondragon Unibertsitatea, Loramendi 4, Arrasate-Mondragón 20500, Spain*
[d]*Manufacturing and Automation Research Center, Koc University, Istanbul 34450, Turkey*
[e]*Sobelcomp SPRL. Rue de l'économie 13, 4431 Loncin, Belgium*

* Corresponding author. *E-mail address:* matthias.nutte@umons.ac.be

Fiber-reinforced polymers (FRPs) are high-performance materials used in lightweight and high-strength applications. Machining is often required because FRP manufacturing processes leave excess material that must be removed to meet final geometry, dimensional tolerances and surface quality requirements. The UD-GFRP laminates are produced by resin infusion and contain stitched plies for handling during manufacturing. A semi-automatic image processing method is proposed to separately quantify delamination and fluffing on surface plies. Slotting tests were conducted using a two-flute straight-tooth PCD cutter on a robotic machining setup, with fiber orientations of 0°, 45°, 90°, and 135° and four feed-per-tooth levels. Fiber orientation and milling strategy (up/down milling) strongly affect surface quality, while feed per tooth has a minor effect. Stitching threads also affect the formation of defects. The optimal configuration is up milling at $\theta = 0°$, producing minimal delamination and reduced fluffing. These results show that delamination and fluffing must be evaluated separately for reliable surface characterization

Keywords: Surface-ply defect, Milling, GFRP, Delamination, Fluffing, Uncut fiber

1. Introduction

Although most machining studies focus on Carbon Fiber Reinforced Polymers (CFRPs), Glass Fiber Reinforced Polymers (GFRPs) remain the most widely used FRP materials worldwide. This imbalance is mainly due to the widespread use of CFRPs in applications demanding high strength-to-weight ratio and stiffness [1], particularly in high added-value sectors such as aerospace, aeronautics, and automotive industries [2], as well as their generally higher cost. CFRPs also exhibit a faster market growth trend compared to GFRPs [3]. Nevertheless, improving the machinability of GFRPs remains essential due to their broad industrial relevance.

Machining FRP composites is challenging due to their heterogeneous and anisotropic structure [4]. The absence of plastic deformation results in fracture-dominated cutting mechanisms, leading to defects such as delamination, fluffing (i.e., uncut or partially cut fibers, with or without attached matrix material, protruding from the machined surface), and fiber pull-out, which contribute to high industrial rejection rates. [4]. In orthogonal cutting, five mechanisms have been identified by Sheikh-Ahmad [5]: delamination (type 1), fiber buckling (type 2), fiber cutting (type 3 et 4),and macro-fracture (type 5), all governed by fiber orientation, which therefore dictates the resulting surface integrity. Colligan [6] recommends using a ply orientation parallel to the trimming direction. Many studies investigate machining-induced defects on FRP surfaces, both on surface plies and on surfaces perpendicular to the laminate. Some works focus solely on fluffing to characterize the surface ply [7], [8], while others distinguish several defect classes within the surface ply [6], [9]. Schrab [8] considers delamination and fluffling as related phenomena and treats them as a single defect, evaluating only fluffing on the surface ply.

The objective of this study is to independently quantify delamination and fluffing to characterize the machined surface

10.1016/j.procir.2026.03.091

plies. A slotting operation was performed using a machining robot equipped with a two-flute straight-tooth PCD insert cutter. The influence of fiber orientation θ and feed per tooth f_z on both delamination and fluffing is investigated.

The surface-ply defects are first introduced and classified into several categories. Next, the post-machining characterization methodology is presented, along with the specific indicators used for each defect type (fluffing and delamination). The experimental setup is then detailed, including the machined material (UD-GFRP), the machining strategy, and the cutting conditions. Finally, the results are presented and discussed.

Nomenclature

θ	fiber orientation angle [°]
A_d	total delamination area [mm²]
A_f	total fluffing area [mm²]
a_p	axial depth of cut [mm]
a_e	radial depth of cut [mm]
f_z	feed per tooth [mm/th]
$L_{d,\max}$	maximum delamination length [mm]
$L_{f,\max}$	maximum fluffing length [mm]
S_d	delamination area per unit cutting length [mm²/mm]
S_f	fluffing area per unit cutting length [mm²/mm]
V_c	cutting speed [m/min]
W	evaluation length [mm]

2. Classification of Surface-Ply Defects

Colligan [6] classified surface-ply defects into three primary types: Type I, Type II, and Type III, with a combined Type I/II mode (Fig. 1). Type I delamination is characterized by areas where surface ply fibers are broken and removed below the machined surface, which results in missing fibers along the trimmed edge. Both Type I and Type III delamination share the consequence of creating loose fibers attached to the machined edge, which imparts a "fuzzy" appearance to the surface. Type III, for its part, represents partially attached fibers or cracks that extend parallel to the machined surface. Conversely, Type II delamination is identifiable by uncut fibers that protrude outward from the machined edge. This specific damage is primarily caused by the fibers bending or moving away from the path of the moving tool, subsequently springing back to their original orientation instead of being cleanly cut. Type I/II delamination is a combination of the characteristics observed in the two preceding types.

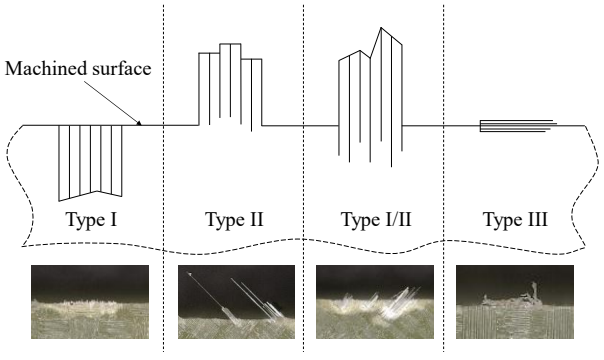

Fig. 1: Schematic representation and illustration of defects (adapted from [9])

From a manufacturing standpoint, Type II and Type I/II defects are highly undesirable because they require manual finishing to remove uncut fibers [9]. In contrast, Type I and Type I/II defects may compromise material integrity by generating subsurface delamination. For these reasons, fluffing (Type II and Type I/II) and delamination (Type I, Type I/II and III) must be quantified separately. Fig. 2 illustrates the differences between fluffing and delamination areas on a slotting test (down-milling side). The boundary between the two defects corresponds to the machined surface (dashed line). The fluffing region corresponds to the uncut parts: fibers and matrix protruding from the machined surface. The delaminated area, on the other hand, is defined by the whitening of the matrix. The feed direction is aligned with the x-axis.

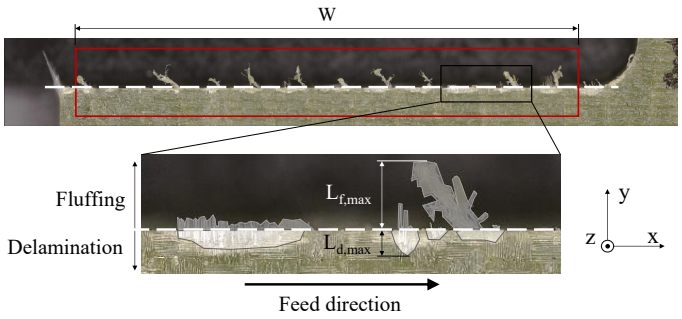

Fig. 2: Fluffing and delamination identification (θ = 90°, f_z = 0.01 mm/th)

3. Post-machining characterization

A Keyence VR-6000 3D profilometer was used to acquire high-resolution images (2453 × 659 pixels, 14.795 µm/pixel) of the entire 35-mm slot. The objective lens used provides a ×40 magnification. Twelve frames were stitched automatically under controlled lighting conditions. Since the viewing direction of the image is normal to the surface, the uncut fibers of the bottom layer interfere with those of the top layers. To avoid this problem, a uniform black background acting as a mechanical filter was placed between the two surfaces (Fig. 3).

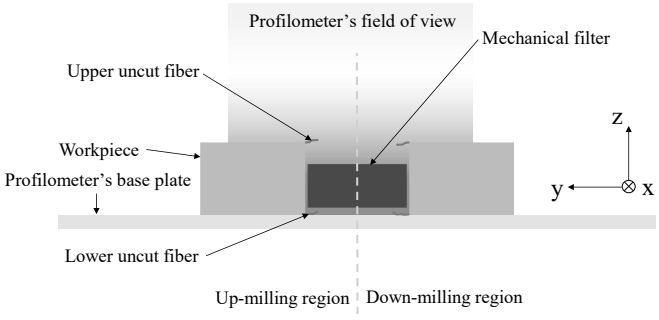

Fig. 3: Field of view of the profilometer and mechanical filter

The acquired 2D images were then processed to identify the fluffing region (or uncut fiber region) and the delamination region. Quantitative indicators were subsequently calculated from the semi-automatically detected areas. The workflow for surface-ply defect characterization is summarized in Fig. 4. The up-milling and down-milling sides of each slot were analyzed separately, since only one edge remains on the final trimmed part. As a result, a global indicator for the whole slot is unnecessary. The defects characterized in the surface ply are

fluffing (or uncut fibers) and delamination.

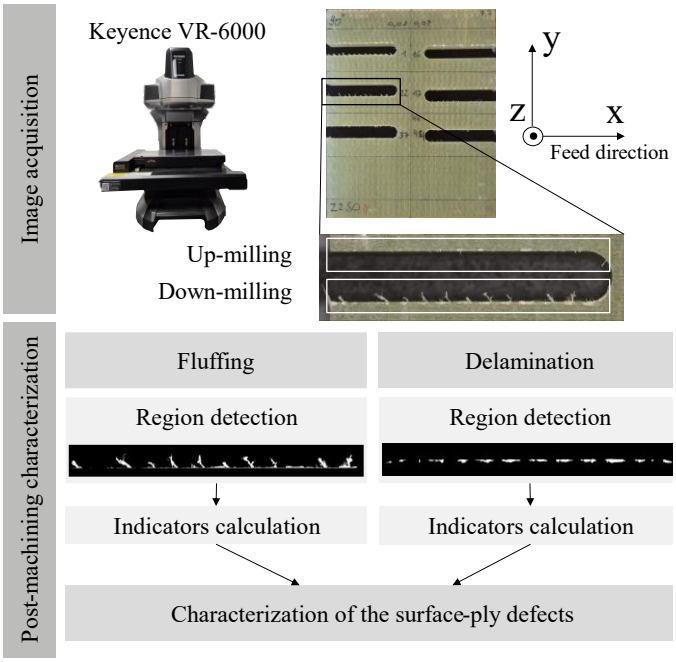

Fig. 4: Surface-ply defect characterization schematic

3.1.1. Fluffing region

The fluffing region is first identified from the acquired image (Fig. 4) before calculating the corresponding defect indicators. The detection process (Fig. 5) is semi-automatic: the region of interest (ROI) is defined manually, including both the study zone of length W (Fig. 2), which excludes the slot entry and exit areas, and the machined surface (dash line in Fig. 2).

From this point, the detection of fluffing regions is fully automatic. Before image processing, the image is leveled based on the inclination of the machined surface using nearest-neighbor interpolation. The image processing pipeline consists of four steps, similar to the approach used by Schrab [8]: conversion to grayscale, noise reduction using a 3×3 Gaussian filter, automatic foreground (fluffing area) detection using Otsu's thresholding, and edge cleaning to prevent non-fluffing regions of the part from being mistakenly included in the fluffing zone. A Laplacian-based sharpness filter is further applied to reject out-of-plane fibers that may bypass both the mechanical filter and Otsu's thresholding: components with insufficient local sharpness — characteristic of fibers outside the focal plane — are systematically discarded.

From the detected region, the maximum fluffing length $L_{f,\max}$ is measured perpendicular to the machined surface (Fig. 2). The fluffing area per unit cutting length S_f is defined as the total fluffing area A_f over the evaluation length W : $S_f = A_f \,/\, W$ [mm²/mm].

3.1.2. Delamination region

Similar to fluffing detection, delamination region detection is semi-automatic (Fig. 5). The initial steps are identical: ROI selection and image leveling. Image processing starts with conversion to grayscale and noise reduction using a 3×3 Gaussian filter. Thresholding is performed empirically. Delaminated areas appear whitened, allowing a grayscale value to identify them. A value of 190 was chosen based on lighting conditions and the material's response.

Morphological operations are then applied to define coherent delamination zones [10]. Two operations are used: opening and closing. Opening, defined as erosion followed by dilation with a 3×3 elliptical kernel, removes isolated noise pixels while preserving genuine delamination features. During erosion, pixels are removed unless all neighbors are white, eliminating clusters smaller than the kernel; subsequent dilation restores the size of legitimate zones without recovering eliminated noise. This conservative kernel size preserves small delamination (5-6 pixels) after Gaussian blur. Closing, defined as dilation followed by erosion with a 5×5 elliptical kernel, unifies fragmented zones and fills internal holes. Dilation bridges gaps of 2-3 pixels and fills voids, while erosion restores original dimensions without reopening filled areas. The larger 5×5 kernel allows aggressive gap filling (up to 3-4 pixels) without merging genuinely separate zones (>5–6 pixels apart).

From the detected region, the maximum delamination length $L_{d,\max}$ is measured perpendicular to the machined surface (Fig. 2). The delamination area per unit cutting length S_d is defined as the total delamination area A_d over the evaluation length W: $S_d = A_d \,/\, W$ [mm²/mm].

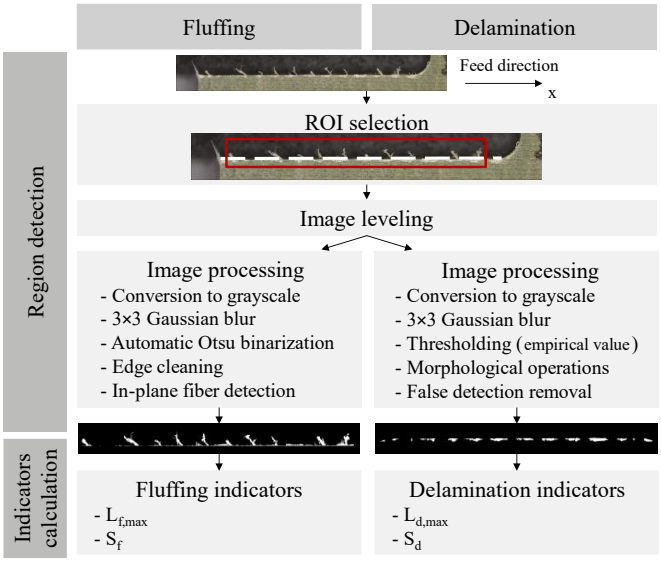

Fig. 5: Defect region detection and indicators calculation schematic

4. Experimental setup

4.1. Workpiece material

A purely unidirectional (UD) GFRP specimen is examined in this paper. The workpieces are UD-GFRP samples provided by Sobelcomp and manufactured by resin infusion. The laminate consists of 14 plies of unidirectional glass fiber tows embedded in an epoxy matrix, all oriented in the same direction. The total thickness of the laminate is 7.3 mm ± 0.2 mm. A transverse cross-section of the specimen is shown in Fig. 6.a. In this view, fibers are perpendicular to the cutting plane, and all 14 plies can be clearly distinguished.

However, although the plies are unidirectional, the handling and formability of parts made from this material require stitching threads to maintain the arrangement of the

unidirectional fiber tows during the infusion process. These stitching threads, highlighted with dashed lines, are illustrated in Fig. 6.b. Their presence influences the formation of defects, since these threads are not oriented in the main fiber direction.

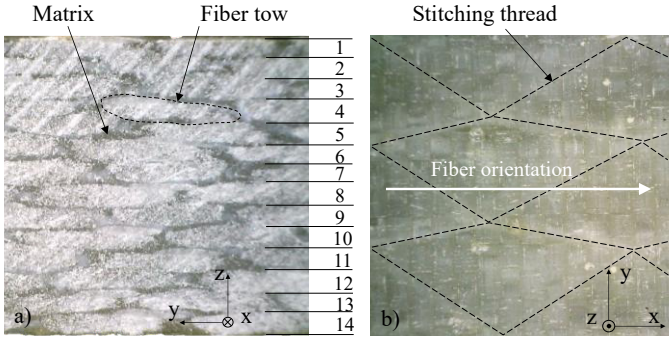

Fig. 6: Cross-sectional view and top view of the specimen

4.2. Robotic machining experiments

The experimental setup is shown in Fig. 7. Slotting tests were performed on a Stäubli TX200 robot equipped with a Teknomotor ATC 71-HSK F63 spindle. The tests were carried out at the UMONS Machine Design and Production Engineering Lab.

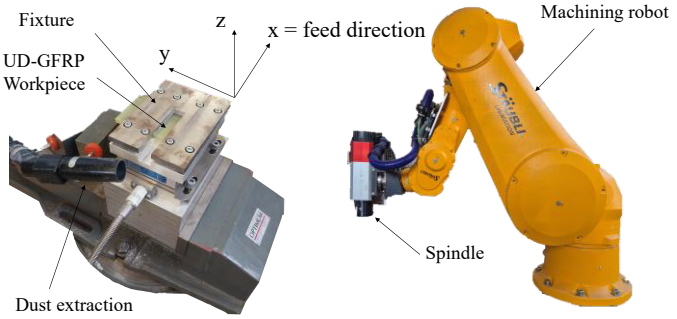

Fig. 7: Experimental setup

The tool studied is a 6 mm-diameter, two-flute straight-tooth PCD milling cutter from Ceratizit (reference 1F400001005-17X) (Fig. 8). It is designed for long tool life when machining non-ferrous metals and plastics. The cutting speed v_c was set to 125 m/min. The axial depth of cut matched the specimen thickness. Only the peripheral teeth participate in the cutting process. Four different feeds per tooth f_z were tested: 0.01, 0.02, 0.03, and 0.04 mm/tooth. Each slotting test was performed over 35 mm in the x-axis (feed direction). The specimens were unidirectional glass fiber–reinforced polymer (UD-GFRP) samples, with the fibers oriented at $\theta = 0°, 45°, 90°$, and 135°relative to the cutting direction. The tests were conducted in a robot posture that maximized structural rigidity [11]. However, this does not exclude the presence of additional dynamic and vibratory effects compared to a conventional CNC machine. Each cutting condition was repeated three times for repeatability.

Fig. 8: 6mm two-flute straight-tooth PCD milling cutter from Ceratizit

5. Results and discussion

5.1. Influence of stitching threads

To facilitate component fabrication [6], surface fibers should be aligned parallel to the trimmed edges along all straight sections. Accordingly, our case study recommends a fiber orientation of 0°. However, it is also in this configuration that the influence of the stitching threads is most noticeable. In principle, Type II and Type I/II defects should not occur because the UD ply is aligned with the cutting direction ($\theta = 0°$). Only Type III defects would normally be expected. The appearance of Type II and Type I/II defects is instead caused by the stitching threads, whose inclination differs from the main ply orientation. Fig. 9 shows such defects for a feed per tooth fz of 0.03 mm/th and a fiber orientation θ of 0°. In both cases, the stitching thread is oriented at 30° relative to the feed direction. An important observation is that portions of matrix remain attached to the uncut fibers. These matrix segments follow the fibers during their deflection: they are not cut by the tool and subsequently undergo elastic spring-back together with the fibers to which they are bonded. As such, these matrix remnants (Fig. 9.a) are classified as part of the fluffing region.

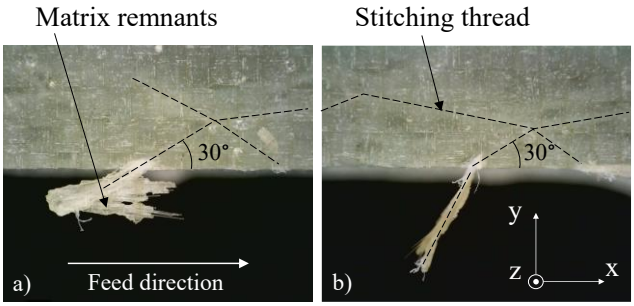

Fig. 9: Influence of stitching threads ($\theta = 0°$, $f_z = 0.03$ mm/th)

5.2. Fluffing region

Fig. 10 displays the fluffing results, showing the mean and standard deviation of three repetitions for each cutting condition. The 45°/down-milling configuration produces both the largest (L_{max}) and the densest (S_f) fluffing. The high level of fluffing observed at 0° is mainly due to uncut stitching threads. Fluffing levels are similar in up-milling and down-milling at 0°. For fiber orientations θ at 90°, up-milling generally minimizes fluffing, while for $\theta = 135°$, and more broadly for orientations greater than 90°, down-milling becomes more effective. This is consistent with the fact that the geometric cutting configuration in up milling for $\theta \in [0°, 90°]$ fis mirrored by down milling for $\theta \in [90°, 180°]$. To compare cutting conditions, only S_f is considered, as it better reflects overall fluffing severity. The maximum fluffing length is less relevant for finishing operations, whereas the density of the defect (S_f) is more critical. For upmilling at $\theta = 0°$, S_f increases with f_z but drops at $f_z = 0.04$ mm/th. For $\theta = 45°$ and 90°, S_f remains nearly constant or decreases as f_z increases. For $\theta = 135°$, S_f steadily increases with f_z. Thus, for orientations between 0° and 90°, a higher feed, such as $f_z = 0.04$ mm/th, helps reduce fluffing. Overall, the most favorable condition for limiting fluffing is observed at $\theta = 0°$, for both

up- and down-milling at low feed rates. In addition, up-milling at $\theta = 45°$ yields good results regardless of the feed rate.

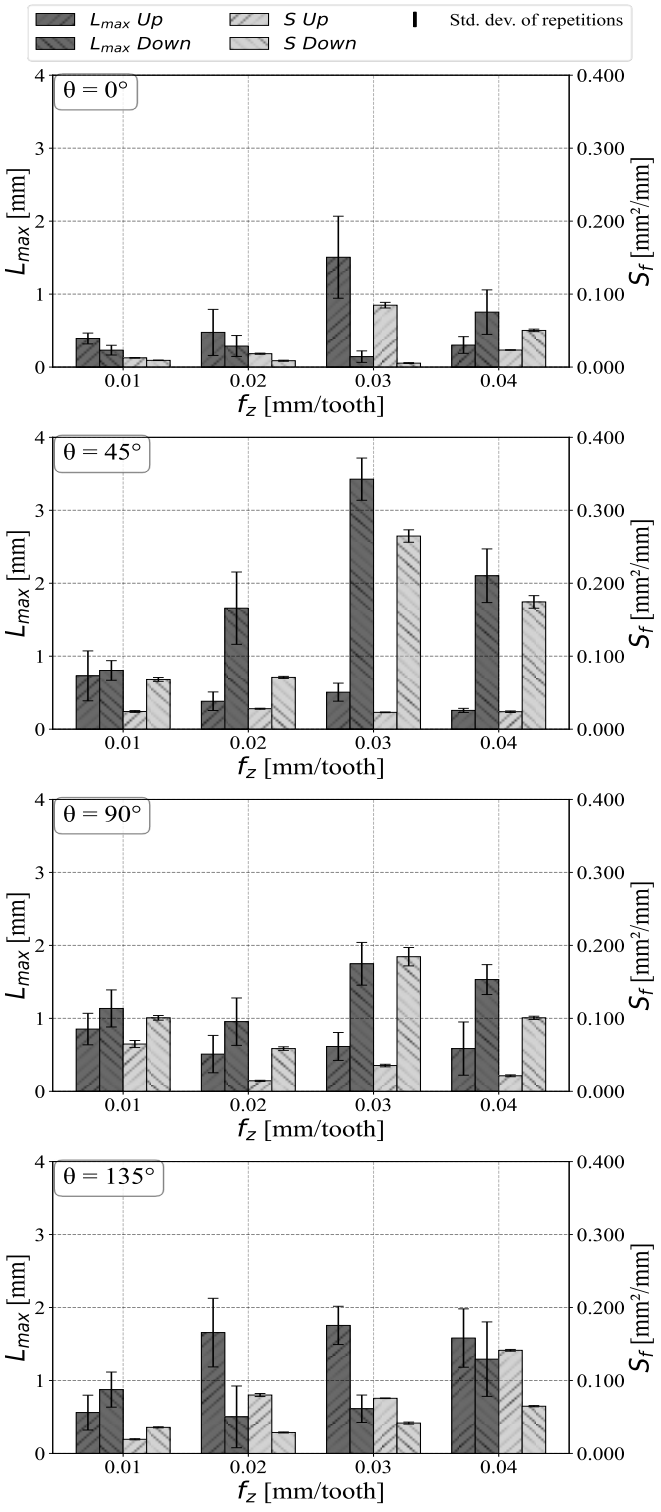

Fig. 10: Indicators for fluffing

5.3. Delamination region

Fig. 11 displays the delamination results, showing the mean and standard deviation of three repetitions for each cutting condition.

At θ = 0°, S_d is of the order of 10^{-2} mm²/mm, i.e. approximately one order of magnitude lower than for the other orientations, independently of the milling strategy. The 135° configuration shows the highest delamination levels, and both 90° and 135° should be avoided as they generate the most severe damage.

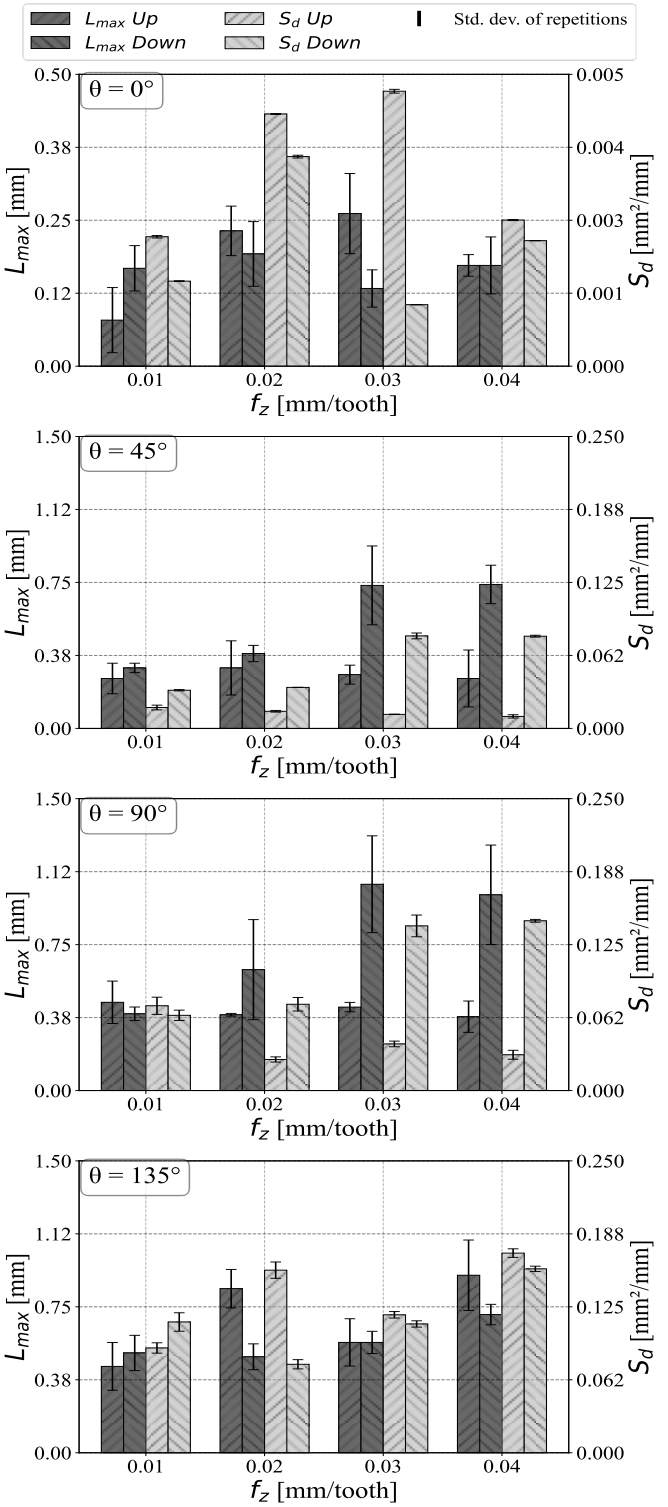

Fig. 11: Indicators for delamination

For $\theta = 0°$ and 135°, no clear difference appears between up- and down-milling. In contrast, for $\theta = 45°$ and 90°, up milling consistently yields lower delamination. For these two orientations, S_d remains roughly constant as f_z increases. Overall, $\theta = 0°$ is the most favorable orientation regarding

delamination. This is consistent with the cutting mechanism: the observed damage corresponds delamination as defined by Sheikh-Ahmad [5]. Fibers separate from each other without propagating damage into the laminate, since delamination occurs parallel to the feed direction.

5.4. Relationship between fluffing and delamination

Similar trends can be observed when analyzing either fluffing or delamination alone, supporting the idea that these defects are related phenomena [5]. However, this correlation does not always hold, particularly for the 0°orientation. In this case, Type II defects are present along with Type III defects induced by the stitching threads. This combination explains the large fluffing lengths observed, despite the very low delamination. For Type II defects, uncut fibers protruding from the machined edge without inducing delamination, it becomes essential to assess delamination separately. Evaluating fluffing alone would mask the fact that the 0°configuration provides excellent surface quality in terms of delamination defect.

5.5. Cutting Strategy for Optimal Surface-Ply Quality

Based on the results presented in sections 5.2 and 5.3, the optimal configuration corresponds to milling with a fiber orientation of $\theta = 0°$. At this fiber orientation, the milling strategy (up- or down-milling) has a limited influence on the results. This orientation strongly limits surface-ply delamination, in agreement with Colligan [6], while up milling reduces fluffing and the need for finishing. The effect of stitching threads is noticeable but minor, due to their non-zero angle relative to the feed direction. Configurations with $\theta = 45°$, 90°, and 135° are not recommended because they produce significant delamination. In general, up milling is preferred for fiber orientations between 0° and 90°, whereas down milling is more suitable for $\theta = 135°$. Fiber orientation and milling strategy have the greatest impact on surface quality, while feed per tooth has little influence (except for $\theta = 135°$). Using the lowest feed ($f_z = 0.01$ mm/th) did not yield the best results, so excessively limiting feed is unnecessary.

6. Conclusion

This study proposed a semi-automatic image processing methodology to separately quantify delamination and fluffing defects on surface plies of machined UD-GFRP composites. The approach enables the independent assessment of both defect types, which is essential since they affect part quality for different reasons: fluffing requires costly manual finishing operations, while delamination compromises the structural integrity of the material.

The experimental investigation using robotic slotting tests with a two-flute straight-tooth PCD cutter revealed that fiber orientation and milling strategy are the dominant factors influencing surface-ply quality, whereas feed per tooth has a relatively minor effect within the tested range. The optimal configuration for minimizing surface-ply defects is up-milling with a fiber orientation of 0° and a feed per tooth of 0.01 mm/th, which strongly limits delamination while maintaining acceptable fluffing levels. Fiber orientations of 90° and 135° should be avoided due to severe delamination.

The presence of stitching threads in the UD fabric was found to induce Type II defects even at 0° orientation, where only Type III defects would otherwise be expected. This highlights the importance of considering manufacturing-related features when predicting machining-induced defects.

Future work will aim to integrate surface roughness measurements into the characterization methodology, providing a more comprehensive assessment of machined surface quality. In addition, cutting forces will be considered to establish correlations with defect formation. By combining roughness parameters with the proposed defect quantification, the relationship between cutting conditions and overall surface integrity can be better understood.

Acknowledgements

The authors would like to thank Région Wallonne for supporting this research as part of the MachFlexComp M-ERA.NET 2022 research project under grant 2210138.

References

[1] J. Zhang, G. Lin, U. Vaidya, and H. Wang, ‘Past, present and future prospective of global carbon fibre composite developments and applications’, *Composites Part B: Engineering*, vol. 250, p. 110463, Feb. 2023, doi: 10.1016/j.compositesb.2022.110463.

[2] Derviş Özkan, Mustafa sabri Gok, and Abdullah Cahit Karaoglanli, ‘Carbon Fiber Reinforced Polymer (CFRP) Composite Materials, Their Characteristic Properties, Industrial Application Areas and Their Machinability’, *Engineering Design Applications III*, vol. 124, pp. 235–253, Mar. 2020, doi: 10.1007/978-3-030-39062-4_20.

[3] Mordor Intelligence Research & Advisory, ‘Glass Fiber Reinforced Polymer Market Size & Share Analysis - Growth Trends & Forecasts (2025 - 2030)’. Mordor Intelligence, Jul. 01, 2025. Accessed: Dec. 15, 2025. [Online]. Available: https://www.mordorintelligence.com/industry-reports/glass-fiber-reinforced-polymer-gfrp-market

[4] M. Altin Karataş and H. Gökkaya, ‘A review on machinability of carbon fiber reinforced polymer (CFRP) and glass fiber reinforced polymer (GFRP) composite materials’, *Defence Technology*, vol. 14, no. 4, pp. 318–326, Aug. 2018, doi: 10.1016/j.dt.2018.02.001.

[5] J. Ahmad, *Machining of Polymer Composites*. Boston, MA: Springer US, 2009. doi: 10.1007/978-0-387-68619-6.

[6] Kevin Colligan and Mamidala Ramulu, ‘The effect of edge trimming on composite surface plies’, *Manufacturing Review*, vol. 5, no. 4, pp. 271–283, Dec. 1992.

[7] A. Hosokawa, N. Hirose, T. Ueda, and T. Furumoto, ‘High-quality machining of CFRP with high helix end mill’, *CIRP Annals*, vol. 63, no. 1, pp. 89–92, 2014, doi: 10.1016/j.cirp.2014.03.084.

[8] B. Schrab, A. Collaine, J.-M. Freyburger, and M. Tourlonias, ‘Machinability analysis of UD-GFRP composites in edge trimming with diamond-coated burr tools at various fiber orientations’, *CIRP Journal of Manufacturing Science and Technology*, vol. 59, pp. 194–206, Jul. 2025, doi: 10.1016/j.cirpj.2025.03.008.

[9] F. Ducobu *et al.*, ‘Sensitivity Analysis of Various Geometries of PCD and Cemented Tungsten Carbide Cutting Tools during the Milling of GFRP Composite’, *Polymers*, vol. 14, no. 8, p. 1524, Apr. 2022, doi: 10.3390/polym14081524.

[10] P. Soille, *Morphological Image Analysis*. Berlin, Heidelberg: Springer Berlin Heidelberg, 2004. doi: 10.1007/978-3-662-05088-0.

[11] F. Ducobu, T. Beuscart, V. Dambly, E. Rivière-Lorphèvre, G. Ortiz-de-Zarate, and P.-J. Arrazola, ‘An experimental methodology to improve the robotic drilling of aluminium alloys’, *CIRP Annals*, vol. 74, no. 1, pp. 103–107, 2025, doi: 10.1016/j.cirp.2025.03.028.